

Optimization of Peak Kilovoltage and Spectral Shape for Digital Mammography

Rebecca Fahrig, Andrew D.A. Maidment and Martin J. Yaffe

Medical Physics Research, Sunnybrook Health Science Centre, and
Department of Medical Biophysics, University of Toronto, Toronto, Ontario M4N 3M5

ABSTRACT

X-ray mammography is one of the most demanding radiological techniques, simultaneously requiring excellent image quality and low dose to the breast. In current mammographic practice, both image quality and dose are found to vary over a wide range of values. Previous attempts to define the optimum operating parameters for mammography systems have been limited due to the lack of realistic attenuation coefficients and absorbed dose data. These data are now available, and have been incorporated into an energy transport model which describes the image acquisition process. The model includes measured x-ray spectra and considers beam filtration, breast thickness and composition, lesion size and composition, scatter, grid transmission and the production and propagation of light in a phosphor-based image receptor. The applied kilovoltage for molybdenum and tungsten target x-ray sources with various spectral filters and average breast composition (50% adipose, 50% fibroglandular) has been optimized with respect to signal-to-noise ratio and absorbed dose and was found to vary between 19 and 29 kVp as breast thickness increased from 4 to 8cm. Preliminary results for various breast compositions and lesions, and experimental verification of the model will be presented. The model may be extended to include either mammographic film or new detector designs for digital mammography.

1. INTRODUCTION

Mammography is the most sensitive and specific imaging modality available for the detection of breast cancer. High performance can only be achieved, however, if the complete imaging system is optimized. In practice, operating factors for mammography are set empirically and vary widely among different facilities. For example, in a survey of 2868 mammographic units in facilities applying to the American College of Radiology (ACR) Mammography Accreditation Program,^{1,2} it was found that the reported kilovoltage used for a typical examination varied from 22 to 44 with a mean of 27.1. The scores on the ACR accreditation phantom, used as an indicator of mammographic image quality, varied (for facilities using a single type of film-screen combination) from 2.0 to 5.4 with a mean of 4.3 for the task of detecting nylon fibers and from 2.0 to 4.8 with a mean of 3.3 for detection of calcific specks in the phantom. In a smaller survey carried out in Ontario, Canada, the same wide range of kVp and image scores was observed as well as a range of entrance skin exposures to the breast of 150 mR to over 1000 mR per image. Although other factors such as film processing presumably account for part of this variation in image quality, it is likely that the wide range of x-ray spectra used is in part responsible.

It is our goal to develop a method for optimizing mammographic imaging techniques, both for conventional film-screen imaging and for digital mammography. Our approach is through an energy transport model of the propagation of signal and noise through the imaging system. The computations make use of experimentally-determined data wherever possible so that the number of assumptions in the model can be minimized. In this paper, we describe the model and present some experimental work to test its validity. We apply the model to the optimization of a prototype digital mammography system.

2. METHODS AND MATERIALS

2.1 Optimization criterion

One of the key problems in optimizing an imaging system is to determine the variable to be optimized. In film-screen imaging one unquestionable goal is to obtain enough transmitted radiation at the image receptor to provide an adequately exposed image, i.e. the desired optical density on the film. Once this requirement has been met, the optimization is generally considered to be a matter of obtaining the greatest contrast over all relevant areas of the breast with the lowest compatible dose to the breast. Since the characteristic display curve for film is nonlinear, contrast is dependent not only on the x-ray spectrum, but also on the level of light exposure to the film at each point in the image. This problem will be dealt with in a future publication.

In digital mammography, the signal from the receptor can be amplified to provide any desired amount of energy to the

next stage of the imaging system and, therefore, the operating exposure is not determined by energy requirements. As well, the characteristic curve of the detector is either linear or can be easily linearized and image contrast can be enhanced as desired at the display stage of the system. The ability to detect an object will be related primarily to the spatial resolution of the imaging system, which is not usually highly energy dependent, and to the signal-to-noise ratio (SNR), which is determined by the energy-dependent contrast and noise properties of the imaging system. We have, therefore, chosen to use the SNR as an index of image quality in digital mammography and as the endpoint in our optimization.

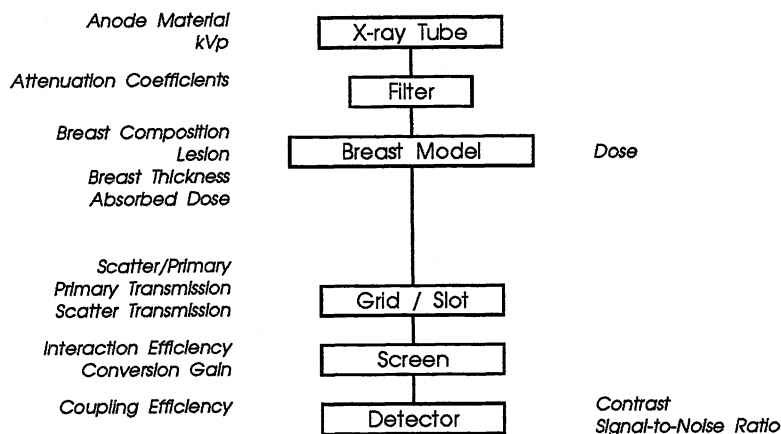


Figure 1. Block diagram of model for mammographic optimization.

2.2 Description of the model

Our model is illustrated in block form in Figure 1. The "raw" (pre-filtration) x-ray spectra were obtained from two sources and combine both measured and calculated data. The molybdenum spectra (e.g. Fig. 2a) are based on the bremsstrahlung model developed by Tucker et.al.³ with added characteristic radiation according to measured spectra provided by Jennings⁴. The tungsten spectra (Fig. 2b) have been interpolated from spectra also measured by Jennings. All spectra have inherent filtration of approximately 1 mm of beryllium. Tube output values for tungsten were measured for a Machlett Model 68KB mammography tube.

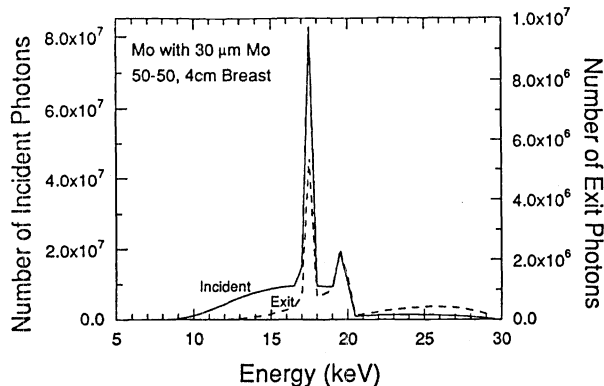


Figure 2a Typical molybdenum target x-ray spectra incident on breast and image receptor.

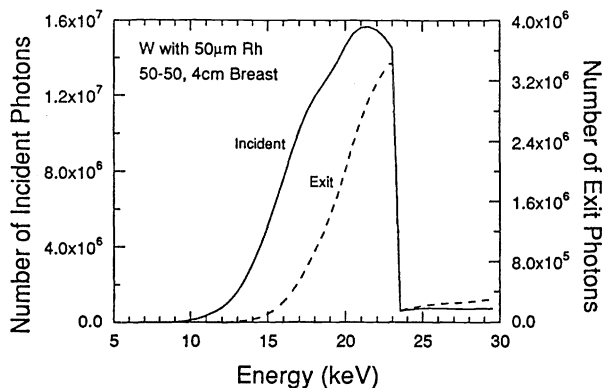


Figure 2b Typical tungsten target x-ray spectra.

The required elemental attenuation coefficients for all materials except the breast tissue were taken from Plechaty et.al⁵. Attenuation coefficients for the x-ray spectral filters and the compression plate, etc. were calculated from their chemical formulae according to the fraction by weight of each element. Beam filtration was varied by the addition of metallic k-edge filters according to target type and detection task.

The breast model shown in Figure 3 is based on the assumptions used by Wu and Barnes⁶ for the calculation of absorbed dose. Their model includes a 0.4 cm thick skin layer (modeled by adipose tissue) surrounding different uniform compositions of breast tissue ranging from 95% adipose-5% fibroglandular to 100% fibroglandular. All of the simulations presented here were performed for a 50-50 composition. Attenuation coefficients for adipose, fibroglandular and infiltrating ductal carcinoma tissues were interpolated using measured data from Johns and Yaffe⁷ and the calcification is assumed to have the attenuation properties of hydroxyapatite⁸ with a density of 3.2 g/cm³. The breast has a semi-circular cross section with a radius of approximately 12.7 cm, providing a large-sized scatter field of 254 cm². Mean glandular dose values were calculated by appropriately weighting monoenergetic normalized dose per incident photon data from the Monte Carlo simulations of Wu et.al. (1991)^{9,*}

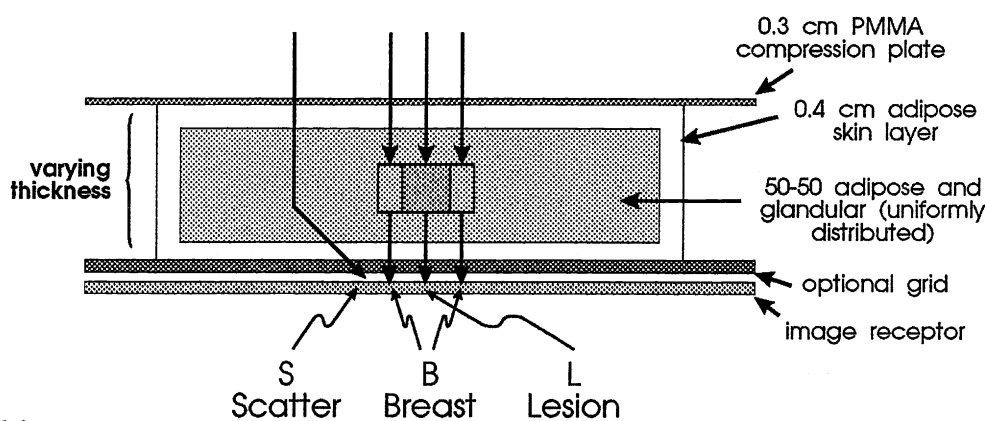


Figure 3 Breast model.

Energy-dependent scatter-to-primary ratios for an area detector were taken from the Monte Carlo simulations performed by Dance and Day¹⁰ for a phantom consisting of equal parts by weight of fat and water at four breast thicknesses, assuming a medium-sized breast field of 93 cm². Although the field sizes for dose and scatter calculations do not correspond, Dance and Day point out that for a 6 cm breast, the scatter-to-primary ratio increases by only 7% when the breast area increases from "small" to "large" at an energy of 25 keV, indicating that dependence on the area of the compressed breast is small. Scatter-to-primary ratios for the scanning slot system were measured in our laboratory, as were the transmission values of the mammographic grid for the breast thicknesses of interest. Both values were assumed to have little variation with energy and thus would not change the distribution of the primary and scatter spectra in the simulation.

The image receptor is modelled in terms of its energy-dependent efficiency of x-ray detection¹¹, the number of secondary quanta produced as a function of energy¹², the statistical fluctuation in this number¹², the signal coupling efficiency between stages and any additive noise sources associated with the detector. Scatter and primary x-ray photons have different interaction efficiencies¹¹ due to the increased pathlength of the radiation in the detector and the slight decrease in x-ray photon energy due to scattering, thereby increasing the relative contribution of scattered radiation to the total detected signal and the noise.

* Wu et.al. found that their breast tissue attenuation coefficients correspond closely to those measured by Johns and Yaffe.

2.3 Signal-to-noise ratio

The model predicts the detection of a cubic lesion surrounded by an annular shell (background) of breast tissue. The lesion was considered to be either a carcinoma or a calcific particle. The signal-to-noise ratio is calculated over equal areas of lesion and background.

The propagation of noise through the system is modelled following the theory presented in Yaffe and Nishikawa¹³. The x-ray source is Poisson distributed, and detector interactions are modeled as Bernoulli processes, with the statistics of secondary quanta formation as described by Swank¹⁴. Transmission of light through lenses is modelled as a simple Bernoulli process. The model currently analyzes the image at zero spatial frequency, however, spatial-frequency dependence will be incorporated shortly.

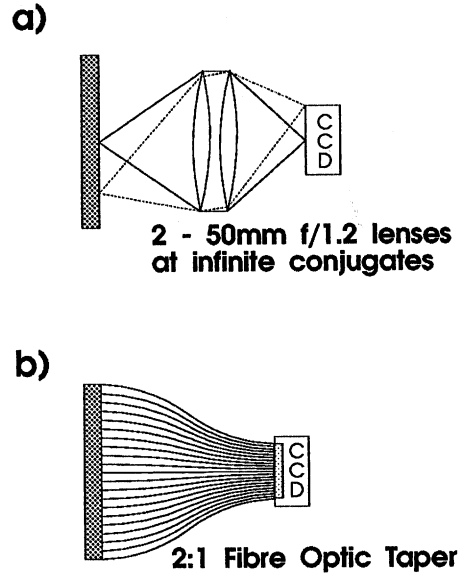


Figure 4 Detector configuration for: a) experimental validation; b) simulation of a digital mammography receptor.

If over a fixed area of the image in the shadow of the lesion the image receptor output arising from unscattered x-ray quanta of energy E in the x-ray spectrum is L_E and the output for an equal area of background is B_E , then the contrast is given by:

$$C = \frac{\sum_E ((B_E + S_E) - (L_E + S_E))}{\sum_E (B_E + L_E + 2S_E)} \quad (1)$$

and the SNR is obtained as:

$$SNR = \frac{\sum_E (B_E + S_E) - (L_E + S_E)}{\sqrt{\sum_E (\sigma_{B_E}^2 + \sigma_{L_E}^2 + 2\sigma_{S_E}^2) + \sigma_D^2}} \quad (2)$$

where S_E is the scattered x-ray contribution to the recorded output, which is assumed constant over lesion and background, and σ denotes the standard deviation in each component. The intrinsic noise from the detector is contained in σ_D^2 . Note that since the scatter component cancels in the numerator of Equation (2), its effect is to decrease SNR because of the presence of $\sigma_{S_E}^2$ in the denominator.

In a slot beam scanning system, where image acquisition times can be significant, two further parameters must be taken into account in the optimization: scan time and tube loading. These parameters have been incorporated by calculating the minimum scan time as a function of heat units required, and by limiting the tube current as a function of applied tube kilovoltage for the two target types.

3. EXPERIMENTAL VERIFICATION

In order to verify the ability of the model to calculate contrast and signal-to-noise ratio, the detector configuration illustrated in Figure 4a was used to acquire images of a 400 μm thick rectangular bone sample¹⁵ on a 12.5 x 12.5 x 6cm thick slab of breast phantom material. The bone samples were obtained from bovine cortical femur and were cut to high precision on a dicing saw. The receptor consists of a gadolinium oxysulfide phosphor screen (Kodak min-R Regular) coupled through 1:1 lenses to a CCD detector¹⁶. This yielded a coupling efficiency of only 17% but provided flexibility in the experimental verification of the model. Exposures were produced on a high frequency x-ray generator, with reproducibility of ± 0.2 kVp and 0.5% of the mAs setting. The mAs was adjusted to maintain constant background signal in the images (1.5×10^8 e⁻/mm² above the dark signal) while camera integration time was held constant to avoid changes in dark noise contributions (dark noise = 8.2×10^3 e⁻/mm²). All images were corrected for pixel-to-pixel variations in offset and gain of the CCD. Images were obtained by irradiating the full area of the phantom to allow verification of large field scatter-to-primary assumptions in the model.

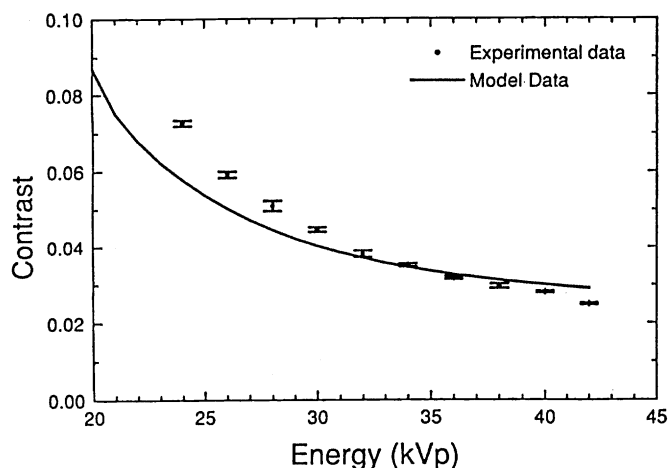


Figure 5a Comparison of predicted and measured contrast.

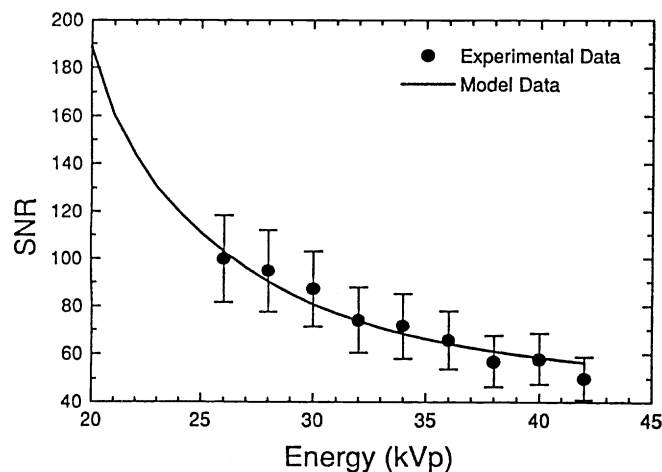


Figure 5b Comparison of predicted and measured SNR

This preliminary version of the simulation does not yet include spatial frequency information and, therefore, the signal-to-noise ratio was calculated over a region of interest (ROI) of 1.2 mm² in the experimental images to ensure that the MTF and noise power spectra approximate their zero spatial frequency values. The signal from six ROIs per image in both background and "lesion" was used to calculate mean and standard deviation and from them, the contrast and SNR according to Equations (1) and (2). Plots of measured and predicted values for contrast and SNR at applied kilovoltages ranging from 24 to 42 are shown in Figures 5a and 5b. Typically, the standard deviation in contrast was 1.5% and in SNR was 13%. Calculated contrast was found to be 25% below measured values. We believe that this is likely due to differences in scatter and in the composition of bone assumed in the model. For comparison purposes the experimental and measured contrasts were matched at 30 kVp and show similar trends with energy. Similar agreement with energy was also found between measured and calculated SNR.

4. SIMULATIONS

Calculations of SNR were performed for a variety of x-ray spectra on a simulated imaging system consisting of a min-R screen coupled via a 2:1 demagnifying fiber optic taper to a frame transfer CCD equipped with a fiber-optic faceplate, as shown in Figure 4b. In spite of the demagnification, the overall coupling efficiency for light transfer in this configuration was 22%. Calculations of SNR over the lesion area were performed for a constant mean glandular dose to the breast of 0.6mGy (60 mrad), a value typical for non-grid techniques in film-screen mammography. This allows comparison of different spectra for constant radiation risk. Except where mentioned, all investigations were performed for a cubic lesion of infiltrating ductal carcinoma of dimension 0.5 cm in a 50-50 breast for thicknesses of 4, 6, and 8 cm.

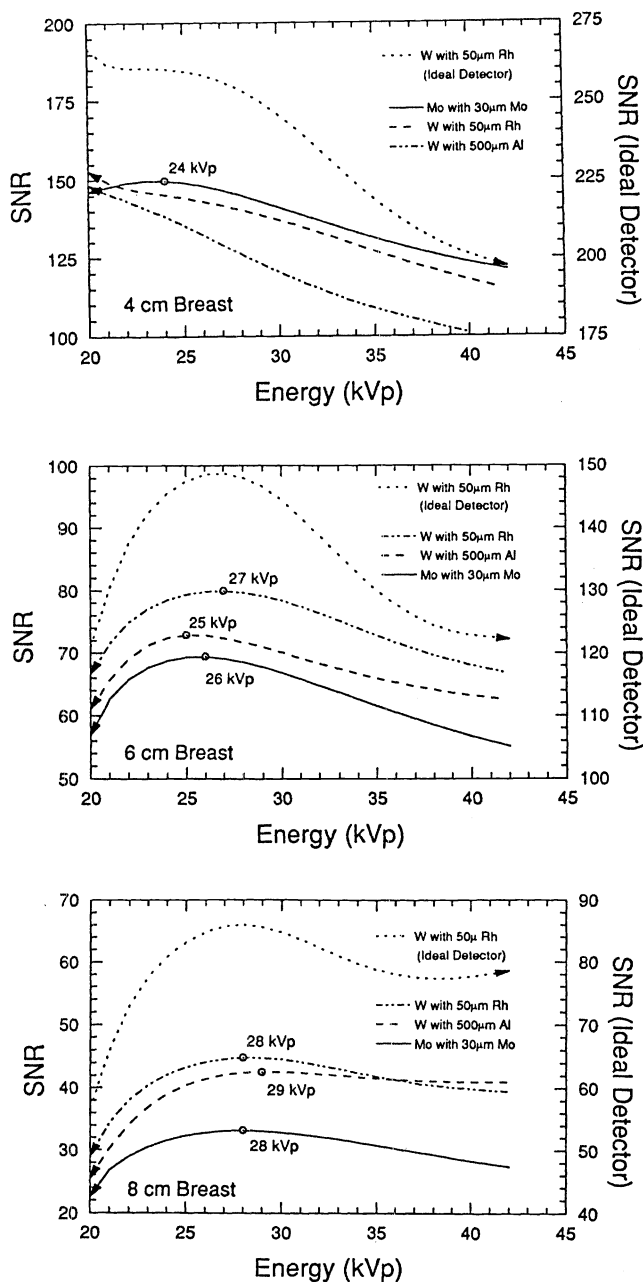


Figure 6 SNR versus applied kilovoltage for detection of 0.5 cm infiltrating ductal carcinoma in 50-50 breast tissue. imaged with optimum SNR (at a given dose) at 34 kVp. However as mentioned above, a 0.5 cm infiltrating ductal carcinoma necessitates a much lower applied kilovoltage, less than 20 kVp with this target/filter combination. A tradeoff between the requirements of the two imaging tasks is, therefore, necessary to ensure adequate visualization of both of the potential indicators of cancer. For molybdenum, the optimum kVp shows less variation, being 25 kVp for the calcification and 24 kVp for the tumor.

4.1 Dependence on breast thickness and lesion - area detector

We present in Figure 6 results for three spectra incident on the detector described above. The molybdenum target spectrum, filtered with 30 µm of molybdenum, is typical of that used in current film-screen mammographic examinations. The tungsten spectrum filtered with 50 µm of rhodium has been suggested by Desponds et.al.¹⁷ as an appropriate compromise between image quality and mean glandular dose according to their Image Quality Index, which is based on statistical decision theory. From calculations performed in our laboratory for monoenergetic x-ray beams, we found that an energy of 21 keV yielded the maximum SNR for a fixed dose (6 cm 50-50 breast, 0.5 cm infiltrating ductal carcinoma). Addition of rhodium filtration to a tungsten target spectrum heavily attenuates both low energy x rays and those above the k-edge of rhodium at ~23 keV thereby making the spectrum more monoenergetic (ie. tuning it to the desired energy). We also performed calculations for a tungsten target, aluminum filter combination. In addition, the SNR for the W/Rh combination is calculated for an ideal energy-weighted detector, i.e. one which has 100% quantum efficiency and which adds no intrinsic noise to the image.

In comparing the results for the ideal detector versus the more realistic detector considered in the model it is evident that there is significant potential for improvement in SNR performance if the detective quantum efficiency can be improved.

From an examination of the trends with respect to breast thickness, several observations can be made. First, for all breast thicknesses, there is some kilovoltage at which the W/Rh combination performs better than the Mo/Mo combination. For the 4 cm breast this is below 21 kVp and in this range most tungsten target x-ray tubes have very low output. The improvement in performance of the W/Rh combination relative to Mo/Mo increases with increasing breast thickness. Secondly, the optimum kVp increases with breast thickness, particularly for the molybdenum target. Finally, for very thick breasts, the SNR curves appear to level off for the tungsten spectra. This implies that the signal and noise are decreasing at the same rate with kVp.

A comparison of the above three spectra for two different lesions (Figure 7) complicates the choice of applied kilovoltage. For the W/Rh spectrum, a 300 µm calcification in a 4 cm breast is imaged with optimum SNR (at a given dose) at 34 kVp. However as mentioned above, a 0.5 cm infiltrating ductal carcinoma necessitates a much lower applied kilovoltage, less than 20 kVp with this target/filter combination. A tradeoff between the requirements of the two imaging tasks is, therefore, necessary to ensure adequate visualization of both of the potential indicators of cancer. For molybdenum, the optimum kVp shows less variation, being 25 kVp for the calcification and 24 kVp for the tumor.

4.2 Slot scanned system

When the receptor is used in a slot-scanning system, tube loading constraints must be considered. For this simulation the same detector technology is used (Figure 4b), but the breast is irradiated with a long narrow x-ray beam and the transmitted radiation passes through a narrow pre-detector slit to impinge upon the screen. The image is acquired over several seconds by scanning the x-ray beam and the detector across the breast from the chest wall to the nipple. The scatter rejection of this system is extremely efficient due to the fore and aft collimators which restrict the beam width to 0.3 cm. In previous work¹⁸ we determined the scatter-to-primary ratio for this geometry for a 6 cm breast to be 0.047 (assumed to be independent of energy). The x-ray tubes considered in the simulation were a Mo target tube with 10 kW rating on the large focal spot and a W target tube with a 45 kW rating. Both tubes had anode capacities of 300 kilo-heat units (kHU).

The simulation was performed using a 6 cm breast and the infiltrating ductal carcinoma as described above. The 6 cm breast thickness represents a reasonably difficult imaging task, in general requiring longer exposure times and, therefore, greater than average tube loading.

Tube loading was modeled by calculating the total number of mAs required per image, based on measured tube output data. The required imaging time was then derived from the instantaneous anode power dissipation limitations, with the tube operating at no greater than 80% of maximum capacity as recommended by the manufacturers. Results are given in Figure 8 for the tungsten target tube and varying thicknesses of rhodium filtration. The plotted SNR values were constrained by the requirement that the total energy deposited in the anode did not exceed the anode capacity of 300 kHU. Tube potentials which allow acquisition of images in less than 8 s and in less than 3 s are indicated. Lower potentials require progressively longer imaging times since tube efficiency drops off.

As more filtration is added, SNR increases but the tube output is reduced due to absorption of x rays in the filter material and greater tube loading is required to deliver a specified patient dose. For that patient dose and for a given scan time (indicated by the solid lines in Figure 8), a peak SNR is reached, and further filtration ceases to provide a gain in image quality. For the tubes modelled here, 10 μm and 30 μm of Rh, both at 32 kVp, give optimal performance for scan times of 3 and 8 s respectively. For comparison purposes, a Mo target with 10 μm of Mo filtration is also shown. Note that due to the lower power rating of the Mo tube, the SNR at 8 s falls well below that provided by the tungsten anode. The exact location of the peaks in the iso-time curves will depend to a large extent on the specific tube under consideration. Adding Rh filtration to the W spectrum leads to an improvement in SNR of 15% over the peak value with the unfiltered beam.

Imaging time is always a concern in scanned beam systems. Shorter imaging times can be achieved by increasing the width of the scanning slot, however, this would increase

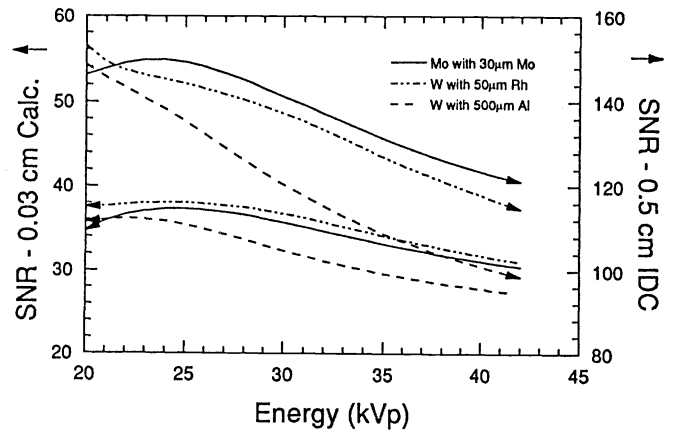


Figure 7 Comparison of optimization for a 5mm cubic tumor and a 300 μm calcification in a 4 cm thick 50-50 breast.

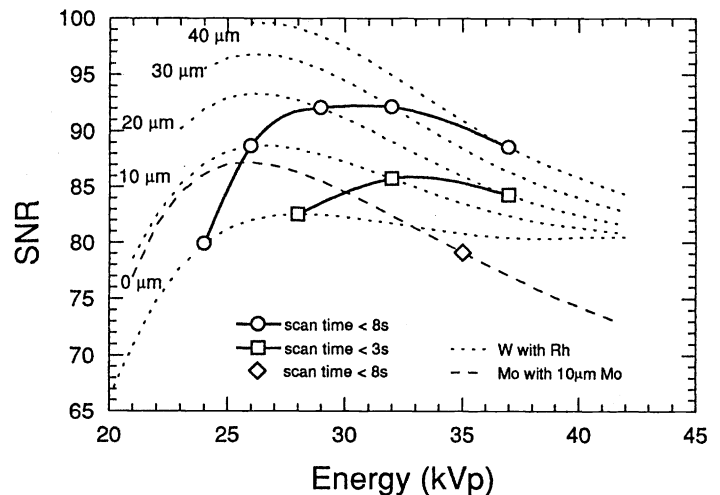


Figure 8 Optimization of scanned-slot digital mammographic detector.

the scatter-to-primary ratio thereby reducing SNR. This optimization will be the subject of further work.

4.3 Effect of anti-scatter grid

We performed a preliminary examination of the use of grids in digital mammography by comparing area detectors with and without a grid to the optimized scanning system as determined above. Because the area detectors require only one exposure to obtain the full image, we chose to apply relatively thick filters on both the tungsten and molybdenum spectra, to maximize the SNR in images acquired using this geometry.

As expected the scanning system provides the highest SNR for fixed patient dose due to the efficient scatter rejection of the 3 mm slot (see Figure 9). Even when five times more Rh filtration is added to the x-ray beam of the area detector, the SNR is still below that of the scanned system. Although in a digital system it is not necessary to replace the radiation lost by removal of scatter and attenuation of primary by the grid, the loss of primary does lead to a reduction in SNR if dose to the patient is fixed. In the case modelled here, addition of the grid leads to a 15% decrease in SNR, indicating that the loss of signal due to absorption of the primary radiation is not compensated for by the concurrent reduction in noise due to scatter rejection.

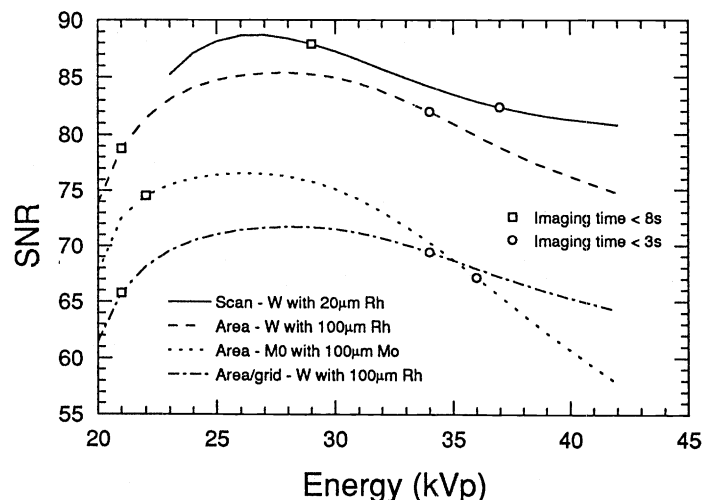


Figure 9 Comparison of area vs. scanned-slot geometries showing the effect of the grid with the area detector.

5. CONCLUSIONS AND FUTURE DIRECTIONS

The existing model predicts the energy dependence of experimentally measured contrast and SNR although discrepancies exist in the absolute values of these quantities. We have shown that for scanned-slot digital mammography systems, the combination of applied kilovoltage and filter material which gives maximum SNR for a specific breast dose and imaging time can be predicted.

For our scanning system geometry, a tungsten target with Rh filtration gives higher SNR at shorter scanning times than is possible to achieve with a molybdenum target tube. For a 6 cm breast and 3 s scan time, peak SNR for a 0.6 mGy dose to the breast is obtained at 32 kVp with 10 μm of Rh.

The high SNR values in our study suggest that it may be possible to reduce patient dose with digital mammography. A comparison of SNR for the two lesion types predicts that detection of calcifications may determine the minimum dose requirement.

For digital mammography systems optimized according to SNR, use of a grid does not appear to offer an advantage. Single and multiple scanning slot systems with air interspace material would seem to be preferable.

This model incorporates data not available to previous investigators^{19,20,21} simulating the mammographic imaging process. We have used measured spectra for both molybdenum and tungsten targets and measured attenuation coefficients for the tissue of the breast and lesion. The availability of monoenergetic absorbed dose data has allowed the comparison of different spectral distributions without the need to assume an average beam energy, and also incorporates any energy dependent effects due to detector interactions. These data also allow consideration of the effects of breast composition and thickness for a wide variety of breast types. The approach is ideally suited for investigation of new detector geometries which may provide improved image quality and for comparison with current technologies.

We plan to extend the model to include spatial frequency analysis and variation in breast and lesion composition. We will also modify the model to deal with the challenging problem of optimization of film systems.

6. ACKNOWLEDGEMENTS

The authors would like to acknowledge the assistance of Dr. Robert Nishikawa, Dr. X Wu, Dr D.M. Tucker, Dr. G.T. Barnes, Dr. R.J. Jennings and Normand Robert for the provision of data. We would also like to thank John Sabol, Sandra Stapleton, N. Robert Bennett and Gord Mawdsley for discussion and help in manuscript preparation. Machlett and Varian Canada provided equipment. This work is funded by the Medical Research Council of Canada and the National Cancer Institute of Canada. The second author is the recipient of a University of Toronto Open Fellowship.

7. REFERENCES

1. R. McLelland, R.E. Hendrick, M.D. Zinninger and P.A. Wilcox, "The American College of Radiology Mammography Accreditation Program," *AJR* 157, pp. 473-479, Sept. 1991.
2. P.A. Wilcox, *private communication*.
3. D.M. Tucker, G.T. Barnes, and X. Wu, "Molybdenum target x-ray spectra: a semiempirical model," *Medical Physics* 18(3), pp. 402-407, 1991.
4. Jennings R J, 1991 *Private Communication*.
5. E.F. Plechaty, D.E. Cullen and R.J. Howerton, *Tables and Graphs of Photon Interaction Cross Sections from 1.0 keV to 100 meV Derived from the LLL Evaluated Nuclear Data Library Vol 6* (Livermore, CA: Lawrence Livermore Laboratory), 1975.
6. X. Wu, G.T. Barnes, and D.M. Tucker, "Spectral dependence of glandular tissue dose in screen-film mammography," *Radiology* 179, pp. 143-148, 1991.
7. P.C. Johns and M.J. Yaffe, "X-ray characterization of normal and neoplastic breast tissue," *Phys. Med. Biol.* 32(6), pp. 675-695, 1987.
8. I. Othman, N.M. Spyrou, J.L. Price and N.M. Gibbs, "Ultrastructure and composition of breast calcification using electron microscopy and microprobe analysis," *Euroanalysis III*, Dublin 1978.
9. X. Wu, G.T. Barnes and D.M. Tucker, *Private Communications*.
10. D.R. Dance and G.J. Day, "The computation of scatter in mammography by Monte Carlo methods," *Phys. Med. Biol.* 29(3), pp. 237-247, 1984.
11. D.P. Trauernicht and R. Van Metter, "Conversion noise measurement for front and back x-ray intensifying screens," in *Medical Imaging IV: Image Formation, Proc. SPIE*, 1231, pp.262-270, 1990.
12. D.R. Dance and G.J. Day, "The computation of scatter in mammography by Monte Carlo methods," *Phys. Med. Biol.* 29(3), pp.237-247, 1984.
13. M.J. Yaffe and R.M. Nishikawa, "Noise in Radiological Imaging," *Proceedings of AAPM Summer School on the Physics of Diagnostic Radiology*, 1991, in press.

14. R.K. Swank, "Absorption and Noise in X-ray Phosphors," *J. Appl. Phys.* **44(9)** pp. 4199-4203, September 1973.
15. Attenuation coefficients from H.E. Johns and J.R. Cunningham, *The Physics of Radiology, Fourth Edition*, Charles C Thomas, Springfield, Illinois, 1983 pp. 720, assuming a bone density of 1.65g/cm^3 .
16. A.D.A. Maidment and M.J. Yaffe, "Scanned Slot Digital Mammography," in *Medical Imaging IV: Image Formation, Proc. SPIE*, **1231**, pp. 316-326, 1990.
17. L. Desponds, C. Depeursinge, M. Grecescu, C. Hessler and J.F. Valley, "Influence of anode and filter material on image quality and glandular dose for screen-film mammography," *PMB* **36(9)**, pp. 1165-1182, September 1991.
18. M.J. Yaffe, R.M. Nishikawa, A.D.A. Maidment and A. Fenster, "Development of a digital mammography system," in *Medical Imaging II: Image Formation, Detection, Processing and Interpretation, Proc. SPIE* **914**, pp. 182-188, 1988.
19. J.W. Motz and M. Danos, "Image information content and patient exposure," *Med. Phys.* **5(1)**, pp. 8-22, Jan./Feb. 1978.
20. E.P. Muntz, H. Jafroudi, R. Jennings and H. Bernstein, "An approach to specifying a minimum dose system for mammography using multiparameter optimization techniques," *Med. Phys.* **12(1)**, pp. 5-12, Jan./Feb. 1985.
21. I. Brodie and R.A. Gutcheck, "Radiographic information theory: Correction for x-ray spectral distribution," *Med. Phys.* **10(3)**, pp. 293-300, May/June 1983.